

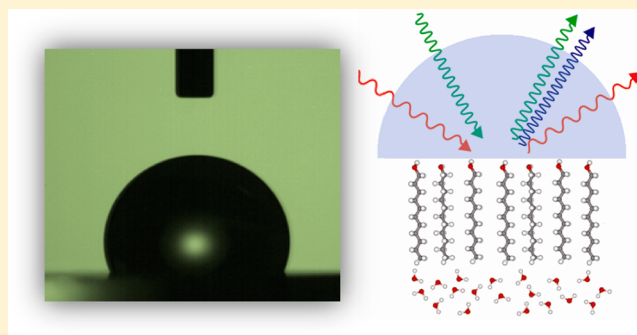
Water Structure Next to Ordered and Disordered Hydrophobic Silane Monolayers: A Vibrational Sum Frequency Spectroscopy Study

Eric Tyrode* and Jonathan F. D. Liljeblad

Surface and Corrosion Science, Department of Chemistry, KTH Royal Institute of Technology, SE-100 44, Stockholm, Sweden

S Supporting Information

ABSTRACT: Vibrational sum frequency spectroscopy (VSFS) has been used to study the structure of water in contact to fused silica surfaces, hydrophobically modified with a series of alkyl trichlorosilane monolayers of varying degrees of order. The interfacial molecular structural information was complemented using total internal reflection (TIR) Raman spectroscopy. The silane molecules consisted of octadecyltrichlorosilane (OTS) and its shorter chain analogue with eight carbon atoms. The VSF spectra show a direct correlation between monolayer order and the intensity of the free OH mode, characteristic of straddling water molecules vibrating in direct contact to the hydrophobic layer, with a concurrent reduction of the bands associated with hydrogen bonded water molecules. The results imply that the structure of water in the most ordered monolayers is not much affected beyond the first layer of water molecules, with bulk isotropic properties becoming apparent already at subnanometer distances from the surface. Contact angle measurements with both water and hexadecane were also performed in an effort to relate macroscopically measurable parameters to the molecular surface structure provided by VSFS and TIR Raman. Only the receding contact angles, and in particular those with hexadecane, were found to correlate with the monolayer order. Finally, to obtain an additional insight into the water structure in direct contact to an ordered hydrophobic surface, isotopic dilution experiments with D₂O were also performed. They indicate that the vibrational coupling mechanism of water molecules at the hydrophobized solid/water interface is different from what has been observed at the liquid/vapor interface.



1. INTRODUCTION

Understanding from a molecular perspective the behavior of liquid water next to extended hydrophobic surfaces is of central importance in a diverse range of phenomena, stretching from the phase segregation observed in oil and water mixtures, to the vital mechanisms that control protein folding in aqueous environments.^{1–3} Nonetheless and in spite of its importance, direct experimental molecular structural information remains scarce, mainly due to the difficulties that probing this interface entails. One important result that has emerged in recent years from X-ray^{4–7} and neutron reflectivity^{8,9} measurements, is evidence supporting the presence of a water depletion layer next to buried hydrophobic surfaces, with the gap believed to amount to a fraction of a water monolayer (<1.5 Å).⁶ Spectroscopic techniques relying on second order nonlinear optical effects, which are intrinsically surface sensitive and capable of distinguishing interfacial molecules from those present in the bulk, have provided additional molecular level information.^{10–12} In particular, vibrational sum frequency spectroscopy (VSFS), starting with the seminal work of Shen and co-workers,¹³ has been repeatedly used to target buried hydrophobic/water interfaces.^{14–21} In all these studies two common spectral features have been observed at this interface, indicating first the presence of water molecules with non-

hydrogen bonded or dangling OH bonds in direct contact with the hydrophobic layer, and second, water molecules with a preferred orientation distinct from those in the adjacent bulk, forming hydrogen bonds of varying strength and coordination. Depending on the nature of the hydrophobic medium, however, the dangling OH band is seen to change, apparently red-shifting with an increase in the polarizability of the nonaqueous phase.^{16,17} Variations have also been observed in the broader band characteristic of hydrogen bonded water molecules, which has been interpreted by differences in the ability of the hydrophobic medium to induce order in the interfacial water molecules.¹³

The most frequently used model system for probing the hydrophobic/water interface, not only on VSFS, but also in X-ray and neutron reflectivity, consists of silica surfaces hydrophobically modified by alkyl silane monolayers. The attractiveness of these chemically attached self-assembled monolayers resides in their robustness and ease of preparation.²² However, the quality of the layer formed depends strongly on the preparation conditions. The factors that are

Received: October 30, 2012

Revised: December 13, 2012

Published: December 21, 2012

known to have an influence include the chain length of the silane molecules,^{23–25} reaction temperature,^{24,26} type of solvent,²⁷ substrate cleanliness²⁸ and hydration,²⁹ concentration of the silane precursor,³⁰ relative humidity,^{26,31} and water content.^{32,33} One consequence of this large number of influencing variables is that finding the optimum adsorption conditions for producing well-ordered monolayers is not always obvious. The monolayer quality is usually evaluated measuring the contact angles with water, which only provides a macroscopic description of the system. Molecular information on the monolayer packing order in air can be obtained from spectroscopy techniques including IR,³⁴ Raman,²⁵ and VSFS.^{20,33,35} However, they are not sensitive to small monolayer defects that are only evident when immersed in water. Defects in the layer can expose the charged silicon oxide substrate, altering the water structure in the surface region next to the hydrophobic monolayers, as suggested by recent VSFS studies.^{14,17,20}

In this work we make a systematic comparison of the structure of water in contact with alkyl trichlorosilane monolayers of two different chain lengths (8 and 18), prepared using slightly different protocols to produce layers with varying degrees of order, as evaluated by the presence of *gauche* defects in the alkyl chain. Emphasis is made in correlating the monolayer conformational order with changes in the water interfacial structure. To facilitate the comparison between the different surfaces, the experimental geometry for delivering the incident beams in the sum frequency spectrometer was chosen to maximize the overall response, with a preferential enhancement of the free OH stretching region.³⁶ Furthermore, contact angle measurements with both water and hexadecane were performed in an effort to relate the macroscopic measurable parameter to the molecular surface structure provided by VSFS. Finally, to gain a further insight in the water structure close to the hydrophobic interface, isotopic dilution experiments with D₂O that simplify the OH stretching region by removing intramolecular couplings are also presented.

2. EXPERIMENTAL SECTION

2.1. Materials. Octadecyltrichlorosilane (OTS) was purchased from Merck. Toluene (anhydrous 99.8%), toluene (99.5+ %), hexadecane, and octyltrichlorosilane (C₈TS), were obtained from Sigma-Aldrich. Deuterated *n*-hexadecane-*d*₃₄ and D₂O were obtained from CDN isotopes and Larodan Fine Chemicals, respectively. Besides hexadecane, which was purified by percolation through a column packed with neutral alumina, all other chemicals were used as received. Water was obtained from an Integral 15 Millipore filtration unit (resistivity of 18.2 MΩ·cm and total organic carbon <3 ppb). The IR grade fused silica hemispheres ($R_s < 0.7$ nm and 10 mm in diameter) were custom-made by CVI-Melles Griot. Chromosulfuric acid from Merck was used for cleaning the hemispheres before silanation.

2.2. Vibrational Sum-Frequency Spectrometer. The femtosecond VSF spectrometer has been described in detail elsewhere,³⁶ and will be only briefly outlined here. A Ti:Light-200 oscillator (Quantronix, USA) is used to seed an Integra-HE-7-FS amplifier (Quantronix, USA) which generates a 1 kHz train of ~90 fs pulses, centered at 806 nm with a total output power of ~6.2 W. The tunable IR pulses are produced in a traveling optical wave parametric amplifier HE-TOPAS-C (Light Conversion, Lithuania), pumped with 75% of the total output power from the Integra HE. The remaining 25% is sent to a home-built pulse shaper that produces the bandwidth-

tunable picosecond visible pulse. These two beams are transmitted through an IR grade fused silica hemisphere and overlapped in time and space at the solid/liquid interface using a copropagating geometry. The spectrometer features a high degree of automation, allowing the motorized control of the beam polarizations, IR power, and angle of incidence and emission of the visible and SF beams. The angles of incidence of the IR and visible beams were fixed at 55° and 70°, respectively. This selection of angles maximizes the overall SF response with a preferential enhancement of the free OH stretching region.³⁶ The average powers and beam diameters at the sample position were 4 mW and 150 μm, and 8 mW and 300 μm for the IR and visible beams, respectively. The generated SF signal is spatially and optically filtered before being directed to a spectrometer (Shamrock SR-303i-B, Andor, Ireland) with a CCD detector attached to its exit port (Newton DU971N-UVB, Andor, Ireland). The overall spectrometer resolution was set to be better than 2 cm⁻¹. The acquisition time for each SF spectrum was 10–20 min (1–2 min per IR frequency step). The spectra were normalized by the nonresonant SF response from a gold film deposited on a silica hemisphere identical to those used for the silane monolayers. The exact gold normalization procedure is described in detail elsewhere.³⁶ The absolute intensity units in SF spectra shown below can be directly compared in the different figures, with 1 normalized unit corresponding to the intensity of the strongest band in the SSP spectra for the bare fused silica/water interface.

2.3. TIR Raman Spectrometer. The Raman spectra were collected in a home-built spectrometer briefly described in what follows. A 532 nm CW laser (Laser Quantum, U.K.) is used as excitation source. The polarization of the laser beam directed to the sample is precisely controlled with an external polarizer and halfwave plate. The Raman scattered light is collected using an ultralong working distance objective (Zeiss, LD-Epiplan-NEO, 50x, NA 0.55) attached to a modified upright Axio microscope (Zeiss, Germany). The collimated scattered light is then passed through a long pass filter (Semrock-Razor Edge), an achromatic half wave plate, and a polarizer (Thorlabs), before being finally focused to the spectrometer slit (Shamrock-Andor, Ireland) and detected with a CCD camera (Newton 940-Andor, Ireland). The polarizer ensures that the polarization of the light entering the spectrograph is always vertical, and the halfwave plate allows selecting the polarization component of the scattered light that is to be analyzed: parallel (*x*) or perpendicular (*y*) to the plane of incidence of the exciting laser. The surface sensitivity of the TIR Raman originates from the use of an evanescent wave as excitation source.^{15,37,38} For the measurements presented here, the angle of incidence of the laser source was set to 80°, which for the silica/water interface corresponds to a probing depth of ~77 nm. Note that the same cell and hemispheres were used for the TIR Raman and VSFS measurements.

2.4. Contact Angle Measurements. The measurements were made in a DataPhysics OCA40 Micro goniometer (DataPhysics Instruments GmbH, Germany). Advancing and receding contact angles were measured using the dynamic sessile drop method. Contact angles were determined using the DataPhysics SCA20 software (the advancing and receding contact angles were calculated using the tangent leaning and elliptical fitting algorithms).

2.5. Sample Preparation and Handling. For the silanization procedure, all fused silica hemispheres were cleaned

following the same protocol. The substrates were first soaked in chromosulfuric acid for at least 2 h, rinsed copiously in ultrapure water, sonicated, and finally rinsed once again in water. The hemispheres were then kept in water and dried in a stream of filtered nitrogen just before immersion in the silanization solutions. The solutions, consisting of toluene and the alkyltrichlorosilane (~ 4 mM), were prepared in gastight tubes in a water vapor free atmosphere. Substrates were kept immersed for ~ 12 h in the sealed tubes, and then rinsed several times in toluene, three times in ethanol, and finally placed in an oven at 110°C for 1 h. This general procedure was followed in the preparation of all monolayers studied in this work. The only difference in the protocol was the water content in the solvent. For the preparation of monolayers A, B, C, E, and C₈TS anhydrous toluene was used, while monolayers D, F, and G were prepared with nonanhydrous toluene (99.5+%). Monolayers defined with single letters were prepared using octadecyltrichlorosilane (OTS). Note that only a selection of a total of more than 40 prepared and characterized monolayers are shown in this work.

The measuring cell consisted of a IR grade fused silica hemisphere (5 mm in radius) sealed with a Viton O-ring to the top of a custom-made glass cell. The incoming laser beams in both the VSFS and TIR Raman experiments, were carefully aligned and overlapped at the center of the hemisphere as verified with a white light microscope. Degassed water was injected through a glass capillary positioned a few millimeters below the center of the hemisphere. All measurements were carried out at $21 \pm 1^\circ\text{C}$.

3. RESULTS AND DISCUSSION

Fused Silica/Water Interface. The SF spectra at three different polarization combinations from the bare fused silica/water interface at ambient pH (~ 5.6) are shown in Figure 1.

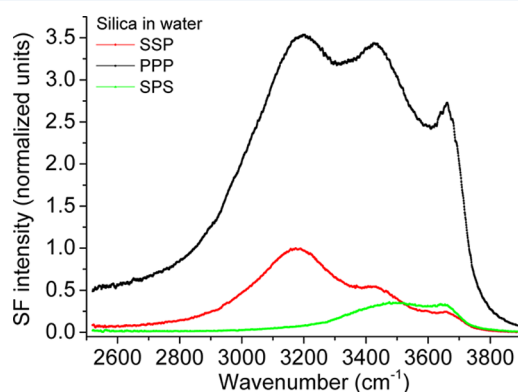


Figure 1. SF spectra of the fused silica/water interface collected in the SSP, PPP, and SPS polarization combinations. The angle of incidence for the IR and visible beams were set to 55° and 70° , respectively. The solid lines are guides to the eye joining consecutive data points.

This particular interface has been the subject of a large number of studies using VSFS,^{39–44} and it is presented here as a reference for the subsequent discussion. At ambient pH, the silica surface is negatively charged due to the partial deprotonation of surface silanol groups.^{45,46} The resulting surface electric field induces a preferred orientation of the dipoles of the interfacial water molecules which can extend over several molecular layers. This induced polar orientation is largely responsible for the observed SF response. In the spectra

shown in Figure 1, three prominent bands can easily be discerned. The first two, centered at $\sim 3200\text{ cm}^{-1}$ and $\sim 3425\text{ cm}^{-1}$ and observed mainly in the PPP and SSP spectra, have been previously identified and associated with water molecules in two different hydrogen bonding environments, commonly labeled as “ice-like” and “liquid-like”, respectively.^{39,41} Recent isotopic dilution experiments^{44,47} however, have put this interpretation in doubt showing that the two bands merge into a single one with increasing HDO concentrations. Notwithstanding, agreement has been found in the presence of an additional band centered at $\sim 3000\text{ cm}^{-1}$ when using both pure water⁴¹ and isotopic dilutions⁴⁷ in phase sensitive SF measurements, suggesting that there is indeed a population of water molecules in the interfacial region forming strong hydrogen bonds. This latter band is not immediately obvious in the spectra presented in Figure 1, but may partly explain the long SF intensity tail extending at low frequencies in the SSP and PPP spectra.

The third band centered at $\sim 3650\text{ cm}^{-1}$ is clearly seen in all three polarization combinations shown in Figure 1. Its relatively high frequency is characteristic of strong OH covalent bonds that are freely vibrating or only very weakly hydrogen bonded. The band could originate from water molecules or surface silanol groups. We have previously observed this band and tentatively assigned it to a Si–OH stretch from silanol groups inaccessible to water molecules.¹⁵ However, experiments performed with deuterated water suggest that this interpretation is not correct since the $\sim 3650\text{ cm}^{-1}$ peak disappears when the silica substrate is in contact with D₂O (see Figure S1 in Supporting Information). We note that this band has not been resolved in the SF spectra presented by others.^{40–44} This difference is partly explained by an improved signal-to-noise ratio, but is mainly a consequence of the experimental geometry chosen for delivering the incident beams, which preferentially enhances the SF response at the high frequency side of the spectrum ($3500\text{--}3800\text{ cm}^{-1}$), making it possible to detect the band.³⁶

Hydrophobized Silica/Water Interface. Figure 2 shows the SSP sum frequency spectra for a number of selected OTS monolayers in contact with water. The spectral window shown includes the CH and OH stretching regions, probing the silane’s alkyl chain conformational order, and interfacial water structure, respectively. In the CH stretching region the two strongest bands are associated with the terminal methyl group, mainly the CH₃ symmetric stretch (r^+) at $\sim 2870\text{ cm}^{-1}$ and its Fermi resonance (r^+_{FR}) at $\sim 2935\text{ cm}^{-1}$, with the exact peak position depending on the monolayer order. The remaining bands in this region are linked to methylene groups in the OTS alkyl chain, in particularly the symmetric CH₂ stretch (d^+) at $\sim 2845\text{ cm}^{-1}$ and its Fermi resonance (d^+_{FR})⁴⁸ at $\sim 2915\text{ cm}^{-1}$, which are only distinctly observed in the spectrum of monolayer D. In SF spectroscopy, the ratio between the amplitudes of the methyl- r^+ , and the methylene- d^+ modes, is used as an indicator of the degree of conformational order in the alkyl chains.^{49,50} In an *all-trans* ordered monolayer the intramolecularly coupled methylene vibrations along the chain are not simultaneously IR and Raman active, rendering the CH₂ modes virtually SF inactive.⁵¹ When *gauche* defects are present, however, the intrachain coupling is lost and methylene modes become detectable in the SF spectra. In Figure 2, monolayer D shows the lowest r^+/d^+ amplitude ratio indicating a conformationally disordered alkyl chain with a large population of *gauche* defects. The remaining three monolayers display significantly

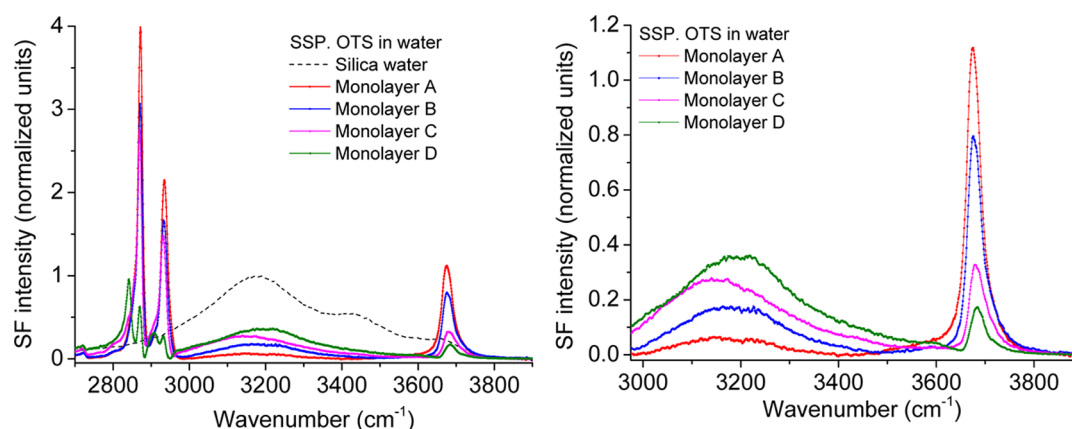


Figure 2. SF spectra of four hydrophobized silica/water interfaces collected under the SSP polarization combination. All monolayers consist of OTS. Left: the SF spectrum for the bare fused silica/water interface is included for reference as a dashed line. Right: Enlargement of the OH stretching region. The solid lines are guides to the eye joining consecutive data points.

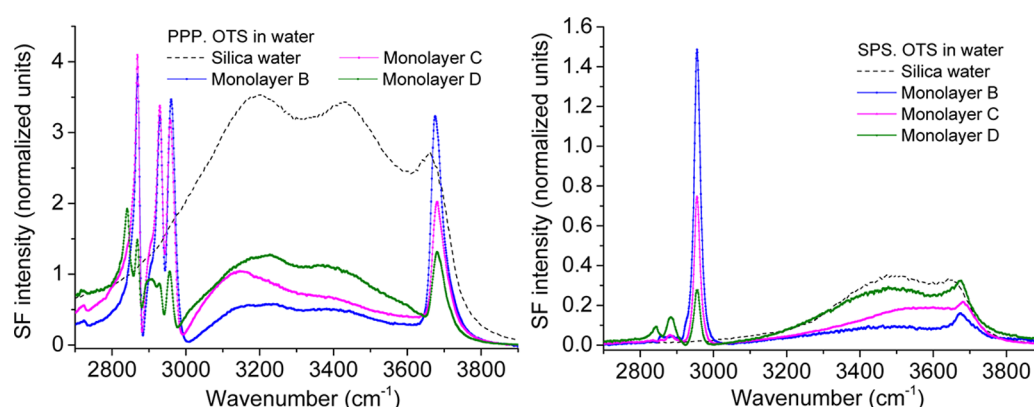


Figure 3. SF spectra of four hydrophobized silica/water interfaces collected under the PPP (left) and SPS (right) polarization combinations. All monolayers consist of OTS. The SF spectra for the bare fused silica/water interface collected at the respective polarization combination is also included for reference as a dashed line. The solid lines are guides to the eye joining consecutive data points.

higher ratios, consistent with close-packed well-ordered monolayers. Nonetheless, differences are still observed in their r^+/d^+ ratios, being highest for monolayer A and B, followed by monolayer C, which shows a small shoulder in the d^+ region (see Figure 5 for details). Notice that the differences in monolayers A, B, and C are due to uncontrolled variables as they were prepared following, in principle, identical protocols.

The other striking feature in the CH stretching region is the variation in the absolute intensity for the same modes in the different monolayers. The SF intensity has a complex dependence on a number of different factors, including the mean orientation of the functional group under consideration, the coherent interference with other signals (notably that from interfacial water), and the number squared of contributing oscillators. The drop in intensity observed in Figure 2 for the different monolayers is primarily due to a broadening in the distribution of angles of the alkyl chains, although for the more disordered monolayer a decrease in the surface coverage will also have an influence. After consideration of these factors, it is evident that from the monolayers presented in Figure 2, the most ordered is monolayer A, followed in sequence by monolayer B, C, and D.

In the OH stretching region of the spectra shown in Figure 2, two main features can be observed: a broad band centered at ~ 3200 cm^{-1} and a sharp band at ~ 3680 cm^{-1} . The latter spectral feature corresponds to the uncoupled OH stretch

mode of straddling interfacial water molecules, having a non-hydrogen bonded OH group oriented toward the hydrophobic surface.^{13,19,20} The peak position of this OH oscillator, referred to as the “free-OH”, is dependent on the nature of the organic phase ranging from 3705 cm^{-1} in air to 3645 cm^{-1} in chloroform, as recently summarized elsewhere.¹⁷ The broad band is characteristic of hydrogen bonded water molecules forming relatively strong hydrogen bonds, as judged by the band’s center position (this interpretation will be reviewed below, after presenting isotopic dilution experiments).

As shown in Figure 2, the two OH bands follow opposite trends with an increase of the monolayer order: the free-OH increases while the broad band becomes weaker. The peak position and bandwidth of the dangling OH oscillator remains, within error, constant (red-shifting, if anything, by less than 2 cm^{-1}). As discussed above, the amplitude rise implies an increasing number of contributing oscillators (i.e., more water molecules having a dangling OH), a narrower distribution of angles for the free-OH bond, and/or, a change in its average orientation.

The other interesting aspect is the reduction of the hydrogen bonded OH band. The presence of this spectral feature at relatively low frequencies has been previously interpreted as the OTS monolayer inducing a more ordered interfacial water structure, when compared to the hydrophobic liquid/water or air/water interface.^{13,16} The results presented here indicate a

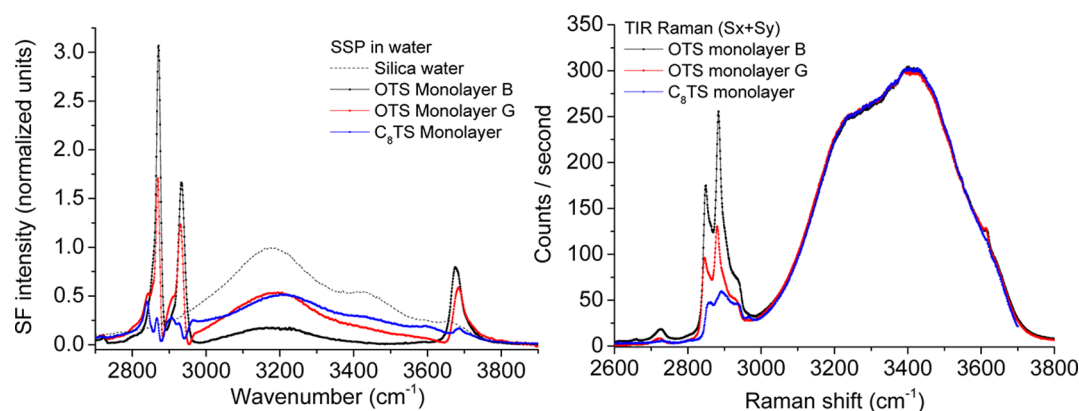


Figure 4. (a, left) SF spectra for three hydrophobized silica/water interfaces collected under the SSP polarization combination. The SF spectrum of the bare fused silica/water interface is also included for reference as a dashed line. (b, right) TIR Raman spectra of the same hydrophobized silica/water interfaces shown in part a collected under the polarization combination $S_x + S_y$. The penetration depth of the evanescent field was set to ~ 77 nm. The solid lines are guides to the eye joining consecutive data points.

rather different scenario. Besides those molecules with a dangling OH in direct contact with the hydrophobic monolayer, the most ordered silane layers appear to induce only a minor preferential orientation of the interfacial water molecules. To discard the possibility that the lack of signal is not due to water molecules adopting an unfavorable orientation not probed in SSP, SF spectra were also collected under the two additional polarization combinations.

In Figure 3 the PPP and SPS spectra for the monolayers B, C, and D are shown. The experimental geometry chosen, that preferentially enhances the spectra at high frequencies, allows resolving the free OH band even in the SPS polarization combination. In the CH stretching region, the antisymmetric CH_3 stretch (ν^-) at $\sim 2955 \text{ cm}^{-1}$ now becomes apparent and dominates the SPS spectra. Moreover, additional bands associated with asymmetric methylene modes,⁵¹ are also discerned in the spectra for the most disordered layer (monolayer D). The intensity variations in the CH bands confirm the conclusions obtained from the SSP spectra, mainly that the most ordered layer is monolayer B, followed by C, and D (PPP and SPS spectra were not measured for monolayer A). Focusing on the bonded OH region, at least two broad bands can be resolved in the PPP spectra centered at $\sim 3200 \text{ cm}^{-1}$ and $\sim 3400 \text{ cm}^{-1}$, while in the SPS spectra the most prominent one is centered at higher frequencies, $\sim 3500 \text{ cm}^{-1}$. This latter band is probably associated with asymmetric water stretching modes,⁵² since the SPS polarization mainly probes off-diagonal elements of the Raman tensor. An additional insight into this region will be gained with the isotopic dilution experiments described further below.

In spite of the differences in the bonded OH region between the different polarizations probed, the general trends regarding spectral changes with an increase in the order of the silane monolayer are consistent. The more ordered layers display the most intense free OH modes, while concurrently, the contributions from hydrogen bonded water molecules decrease to a minimum. The main implication of these results is that the structure of water, beyond the first layer of water molecules in direct contact to the terminal methyl groups, is not much affected by the presence of the hydrophobic surface, with bulk isotropic properties becoming apparent already at a subnanometer distance from the surface. Note that the companion OH oscillator on the straddling water molecules responsible for the free-OH vibration is also expected to have a preferred

orientation and generate a SF signal. This bond, commonly referred to as “donor OH”, is directed toward the bulk of the liquid where it forms hydrogen bonds with other water molecules. The “donor OH” is expected to give rise to a broad band in the $3400\text{--}3550 \text{ cm}^{-1}$ spectral region.^{53–56}

Origin of the Water Bands in Disordered Monolayers.

In contrast to the most ordered monolayers, the spectra shown in Figures 2 and 3 indicate that as the disorder in the monolayer increases, more hydrogen bonded water molecules in the interfacial region adopt a preferred orientation (i.e., disordered hydrophobic monolayers induce a larger structuring of the interfacial water molecules). This interpretation is surprising and requires further consideration. Previous SHG⁵⁷ and VSFS²⁰ studies on OTS monolayers in contact with aqueous solutions of varying pH, have demonstrated that both the second harmonic response and the SF-bonded OH water bands closely followed the behavior observed from the bare fused silica/water interface. These results indicate that most of the effects observed in the bonded OH region are not due to the interactions of water with the hydrophobic monolayer, but instead induced by the underlying fused silica substrate. This interpretation was further developed recently, where it was suggested that substrate access is granted by defects in the SAM and not through penetration of the monolayer alkyl chains.¹⁷ As mentioned above, at natural pH (~ 5.6) the bare fused silica surface is negatively charged, and it is the resulting surface electric field that polar orients the water molecules. Additional evidence showing that the silica surfaces hydrophobized with disordered silane monolayers carry a negative charge, can be found in surface forces measurements using the MASIF instrument.^{58–60} For comparison, note that hydrophobically modified gold surfaces using alkylthiols are uncharged.⁶⁰

Consequently, the presence of intense bonded water bands in the SF spectra is an indication of disordered monolayers or possibly also, ordered monolayers with incomplete surface coverage. To illustrate this latter scenario, the SF spectra for two additional monolayers are shown in Figure 4a. Monolayer G, in spite of showing small shoulders in the spectral regions associated with methylene modes, displays a relatively high r^+/d^+ amplitude ratio indicative of an ordered monolayer with a low population of *gauche* defects. Furthermore, the free OH signal is correspondingly high. However, the bonded OH modes are large, accounting for more than half of the intensity expected for the bare fused silica/water interface (dashed line in

Table 1. Contact Angles in Water and *n*-Hexadecane on Selected Hydrophobized Surfaces^a

	contact angles (deg)					
	water			hexadecane		
	static	advancing	receding	static	advancing	receding
monolayer A	110 ± 1	114 ± 3	106 ± 2	42 ± 1	43 ± 1	34 ± 2
monolayer B	110 ± 1	115 ± 3	106 ± 2	42 ± 1	43 ± 1	31 ± 2
monolayer C	108 ± 2	110 ± 3	95 ± 5	39 ± 1	40 ± 5	26 ± 7
monolayer D	102 ± 2	109 ± 3	71 ± 5	<3	—	—
monolayer E	109 ± 1	111 ± 2	99 ± 4	22 ± 2	22 ± 4	<3
monolayer F	104 ± 4	109 ± 3	92 ± 5	<3	—	—
monolayer G	106 ± 4	116 ± 1	94 ± 2	27 ± 1	30 ± 1	12 ± 3
monolayer C ₈ TS	107 ± 2	110 ± 4	92 ± 2	<3	—	—

^aWith the exception of the C₈TS (octyltrichlorosilane) monolayer, all surfaces were hydrophobized using OTS.

Figure 4a). These spectral features are characteristic of an incomplete surface coverage. OTS monolayers at room temperature are known to grow on the silica surface by first forming domains and islands that eventually expand, covering the whole surface.^{26,33,34} These domains can consist of well packed ordered layers. As mentioned above, however, SF is not ideally suited for determining surface coverage due to its complex dependence on the adsorbed amount. In Figure 4b, the TIR Raman spectra collected under the S_x + S_y polarization combination is shown for the same monolayers as those of Figure 4a. The TIR Raman signal is linearly proportional to the number of molecules per unit area. It also has the advantage of being able to essentially detect all the different functional groups present in the region probed by the evanescent field. In the TIR Raman spectra the dominant features are now, in contrast to the SF spectra, associated with methylene modes, specifically the d⁺ and d[−] modes at ~2845 cm^{−1} and ~2885 cm^{−1}, respectively (note that for OTS there are 17 CH₂ groups compared to a single CH₃ per alkyl chain). A qualitative indication of the conformational order in the silane chain can instead be obtained examining the relative intensities between the d[−]/d⁺ modes, with more ordered monolayers displaying a larger ratio.⁶¹ For monolayer G, this ratio is a fraction lower than for monolayer B, which is consistent with the SF spectra. Moreover, provided there are no major changes in the alkyl chain tilt as can be confirmed from TIR Raman spectra collected at different polarizations,¹⁵ the integrated area below the CH stretching region can be used to estimate the adsorbed amount. When compared with monolayer B, it is clear from Figure 4b that monolayer G has a significantly lower surface number density. This conclusion is in accordance with the SF interpretation of an incomplete surface coverage.

The spectra for the shorter chain silane layer (C₈TS) presented in Figure 4 also show additional interesting features. At room temperature, alkyl silanes with chains shorter than 16 carbon atoms are expected to produce disordered layers regardless of the preparation protocol,²⁴ a fact that is directly confirmed in the SF and TIR Raman spectra. Note that the comparatively lower signals for the CH stretching modes in the TIR Raman spectrum are primarily a consequence of the smaller number of methylene groups in the alkyl chain (i.e., seven in C₈TS compared with 17 for OTS). In the OH bonded region of the SF spectrum, the hydrogen bonded water bands are relatively strong and appear to closely match the general features from the bare fused silica/water interface (dashed line), while the free OH signal is barely distinguishable. This indicates that the water structure next to this interface is dominated by

the underlying silica substrate. Finally, it is worth considering the OH stretching region for TIR Raman to understand the uniqueness of VSFS. The fact that the TIR Raman spectra in all three monolayers closely overlap in the OH stretching region would imply similar water structures in the probed volume (the shoulder observed at 3615 cm^{−1} originates from the bulk silica substrate). At first glance, this appears to be in contradiction to the VSFS results. However, TIR Raman is not suitable for measuring the interfacial water structure. The probing depth of the evanescent field for the TIR Raman experiments is ~77 nm, which indicates that more than 97% of the water probed is actually bulk water since the thickness of the interfacial water (i.e., properties different from those in the bulk) is expected to be in the order of just a few ångströms.

Correlation between Macroscopic Contact Angles and Molecular Structure. Contact angles are frequently used to characterize hydrophobic surfaces, and it is thus relevant to determine if there are correlations with the molecular information obtained from VSFS and TIR Raman. A priori, contact angles, a thermodynamic macroscopic quantity, should not necessarily reflect the interactions that govern molecular orientation and order at interfaces. The contact angles of water and hexadecane on the differently prepared monolayers are summarized in Table 1. The first noticeable point is that the static and advancing angles of water are, within error, practically identical for the different surfaces (only monolayer D shows a significantly lower static contact angle). Noticeable variations are observed, however, in the receding angles, with the most ordered layers showing the highest values and lowest hysteresis. Nonetheless, with the exception of monolayer D, the remaining layers cannot be distinguished solely based on the receding angles of water. Measurements using hexadecane, and in particular receding contact angles, are in this sense far more useful for distinguishing the different substrates, following closely the order determined by the spectroscopy measurements.

Microscopic theories have been put forward to explain the relation between structure and contact angle hysteresis. One of these theories⁶² suggests that the alkyl chains of the chemically grafted monolayer, in particular, the exterior region of the SAM will experience structural changes when in contact with hexadecane or other similar alkanes. VSFS is ideally suited to explore these potential changes. In Figure 5, the SF spectra of monolayer B in contact with water, deuterated hexadecane, and air are shown. The experimental geometry chosen for collecting the spectra is not favorable for the solid/air and solid/d-hexadecane cases, resulting in significantly weaker SF signal.

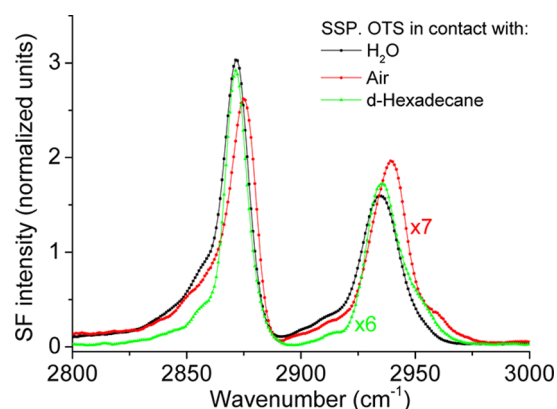


Figure 5. SF spectra of an OTS monolayer (monolayer B) in contact with water, deuterated hexadecane, and air, collected under the SSP polarization combination. For ease of comparison the spectra of OTS in contact with air, and deuterated hexadecane, have been multiplied by seven and six, respectively. The solid lines are guides to the eye joining consecutive data points.

Therefore, the two spectra have been multiplied by constant factors for ease of comparison. The SF spectra for the solid/water and solid/d-hexadecane interfaces show only minor changes, both in terms of peak positions, and overall spectral shape. This implies that no detectable conformational changes occur in the hydrophobic monolayer when removed from water and placed in direct contact with the alkane. The apparent difference in the r^+ / d^+ amplitude ratios, with the d^+ mode at the solid/water interface displaying a higher relative intensity is only a consequence of constructive interference with the broad OH stretching modes from water (a similar situation can be observed when H_2O is exchanged by D_2O as shown below in Figure 7). Furthermore, when in contact with air, the peak positions of both the r^+ , and r^+_{FR} modes blue-shift by $\sim 3\text{ cm}^{-1}$. This change in peak position is reminiscent of the blue-shift of $\sim 20\text{ cm}^{-1}$ observed in the free-OH mode of straddling water molecules for an equivalent change in environment: hydrophobic solid/liquid to the liquid/air interface.

Depending on the monolayer order, the peak positions of the methyl stretching modes were also seen to shift when in contact with water. Figure 6 shows the SF spectra in the CH stretching region of a selection of monolayers in contact with

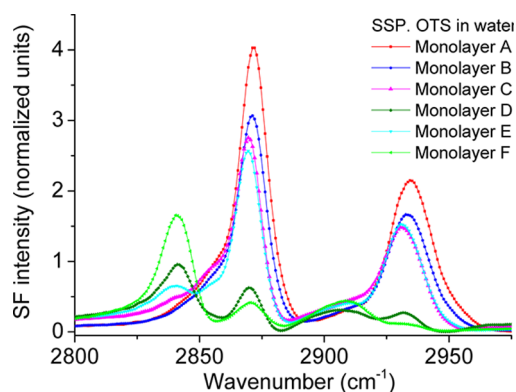


Figure 6. SF spectra of a set of OTS monolayers on silica in contact with water, collected in the SSP polarization combination. Note the dual d^+ signals observed at $\sim 2855\text{ cm}^{-1}$ and $\sim 2840\text{ cm}^{-1}$, respectively. They are simultaneously observed in the spectra of monolayer C and E.

water. The conformational disorder increases from monolayer A to F, which can be inferred from the increasing d^+ intensity accompanied by the decreasing r^+ intensity (*vide supra*). The increasing disorder also results in a small ($\sim 1\text{ cm}^{-1}$) but significant, red-shift of the r^+ and r^+_{FR} peaks, which is most clearly resolved in the spectra of monolayer A to D. This red-shift can presumably be attributed to changes in the van der Waals interaction between the hydrocarbon chains, and/or between the hydrocarbon chains and the adjacent water, analogously to how the red-shift of the free OH vibration in contact with environments of increasing polarizability is rationalized.¹⁷

Moreover, the high resolution spectra shown in Figure 6 allow distinguishing two different d^+ peaks, centered at $\sim 2855\text{ cm}^{-1}$, and $\sim 2840\text{ cm}^{-1}$, respectively. A similar doublet, although at slightly higher wavenumbers, have been observed in the Raman spectra of *n*-hexane.⁵¹ The higher wavenumber band was attributed to the methylene groups next to the terminal methyl group, while the lower wavenumber band was assigned to the methylene stretching mode of the groups in positions 3 and 4. For the most disordered monolayers in Figure 6 (monolayers D and F), only the $\sim 2840\text{ cm}^{-1}$ band can be detected in the spectra. Further, in the slightly more ordered monolayers both bands are observed (monolayers C and E), while in the remaining two layers (A and B) only the high frequency band is resolved. In accordance to the Raman spectra of *n*-hexane, we claim that the $\sim 2855\text{ cm}^{-1}$ band is characteristic of *gauche* defect next to the terminal methyl group, while the lower frequency band is most probably associated with *gauche* defects in the center positions along the chain. This suggests that defects are first observed in the exterior region of the silane monolayer, propagating further down the alkyl chain as the conformational disorder increases.

Isotopic Dilution Experiments Using an Ordered OTS Monolayer. Isotopic dilution experiments with D_2O provide an additional insight into the surface water structure next to hydrophobic monolayers. The presence of partially deuterated HOD prevents intra- and intermolecular vibrational couplings that are known to complicate the interpretation of the SF spectra.^{44,47,55,63,64} Figure 7 shows the SF spectra of monolayer B in contact to neat H_2O , neat D_2O , and a mixture of H_2O and D_2O resulting in a 25:50:25 molar proportions of H_2O :HOD: D_2O .

In the CH stretching region, besides a small blue-shift of the methyl vibrational modes ($\sim 1\text{ cm}^{-1}$) observed in the neat D_2O spectra, no significant changes are detected in any of the three polarization combinations. This finding confirms that the monolayer conformational order is not affected by the introduction of heavy water. In the neat D_2O spectra, it can be noticed that the broadbands that appear in the OH region for the H_2O spectra are no longer present. The isotopic substitution of hydrogen by the heavier deuterium atoms results in the red-shift of approximately 800 cm^{-1} of the equivalent protonated stretching vibrations. The free-OH of H_2O at $\sim 3680\text{ cm}^{-1}$ is observed to shift to $\sim 2713\text{ cm}^{-1}$, and is correspondingly referred to as the free-OD of D_2O . Note that in the SSP spectrum of D_2O a double peak appears in the free-OD stretching region (see inset). The low frequency mode is the free-OD, while the peak centered at $\sim 2725\text{ cm}^{-1}$ is associated with a CH stretching mode of the alkyl chain, tentatively assigned to an overtone of the methyl symmetric bend.¹⁵ This latter mode can also be observed as a shoulder in the PPP spectrum. The bonded OD stretching vibrations are in

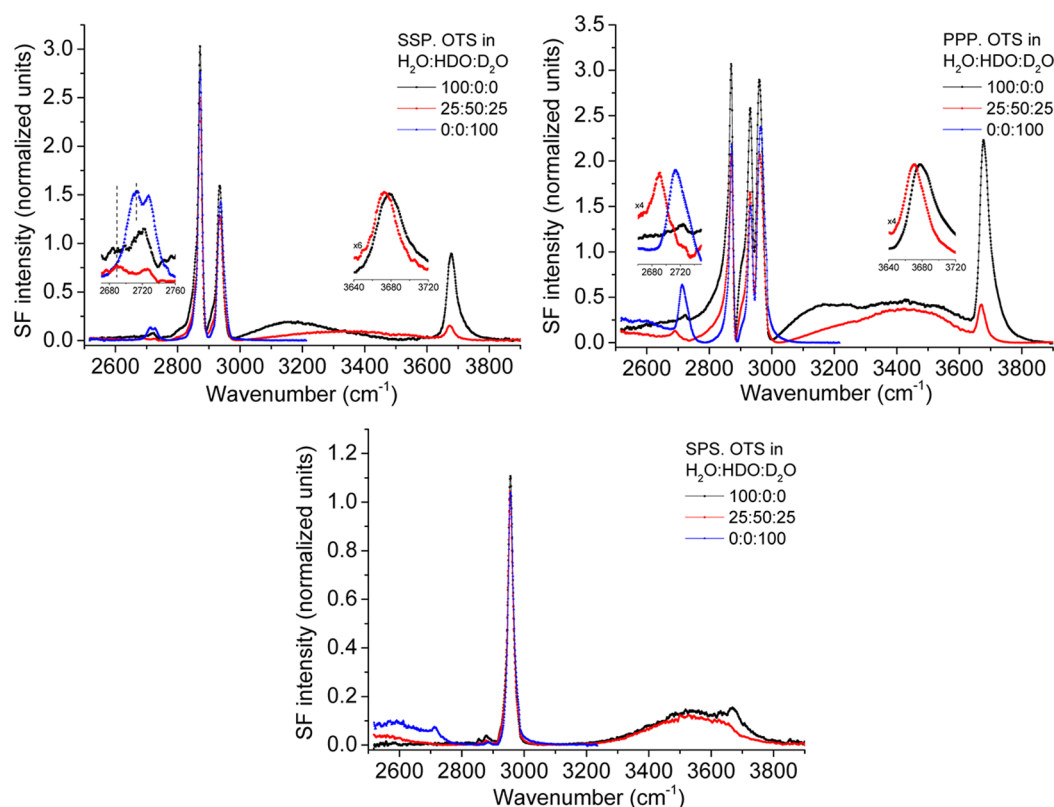


Figure 7. SF spectra of a hydrophobized fused silica substrate (monolayer B) in contact with H_2O , D_2O , and the isotopic mixture 25:50:25 of H_2O :HOD: D_2O . Spectra were collected under the polarization combinations SSP, PPP, and SPS. Insets are included in the SSP and PPP spectra showing the shift in the free-OD and free-OH modes upon isotopic dilution. The solid lines are guides to the eye joining consecutive data points.

turn expected between ~ 2200 and 2650 cm^{-1} . Although the spectra are truncated at 2525 cm^{-1} (the fused silica substrate strongly absorbs IR radiation below approximately 2800 cm^{-1} limiting the accessible frequency window), the end of the bonded OD stretching region can still be clearly observed in the PPP and SPS spectra.

In the spectra of the H_2O : D_2O mixture, where HOD is the dominant species and intramolecular and intermolecular couplings are significantly reduced, interesting features are apparent. Starting with the bonded OH region, the broadband centered at $\sim 3200\text{ cm}^{-1}$ is reduced in the SSP and PPP spectra of the isotope mixture compared to the neat water spectra. In the spectrum this band blue-shifts to $\sim 3350\text{ cm}^{-1}$, suggesting that the actual bond strength of the water molecules forming hydrogen bonds at the hydrophobic silica/water closely resembles those of water in the bulk. As mentioned above, however, the $\sim 3200\text{ cm}^{-1}$ band in the SSP spectra is most probably a consequence of the surface field generated by the underlying fused silica substrate and not from water interactions with the hydrophobic monolayer. In the SPS and PPP spectra the intensity of the broadband centered at higher frequencies ($\sim 3450\text{--}3500\text{ cm}^{-1}$) is only slightly reduced with the center position remaining approximately constant upon isotopic dilution. This band is assigned to the uncoupled “donor OH” vibration from the same straddling water molecules responsible for the free OH vibration,^{53–56} and is consistent with the fact that the band center position is largely unaffected by isotopic dilution. Although expected to remain constant, the intensity of the “donor OH” band relative to the free OH mode, is seen to be significantly higher in the mixture. The apparent discrepancy is mainly a consequence of an

unequal enhancement of the SF signal across the OH stretching region, which significantly varies upon isotopic dilution due to changes in the refractive index of the liquid. This effect is particularly marked for the geometry chosen here to deliver the laser beams.³⁶ Theoretical predictions on how the relative intensities are expected to change across the CH and OH stretching region for different isotopic mixtures and polarization combinations are presented in the Supporting Information (Figures S2, S3, and S4).

Focusing on the free-OH and free-OD modes of the isotopic mixture spectra, two important features are worth considering. First, the amplitudes of the free-OD and free-OH are reduced relative to the neat liquid cases. This is a consequence of (i) the lower number density of the OH, and OD groups in the mixture (note that SF signal has quadratic dependence on the number of contributing oscillators), and (ii) also a reduced Fresnel enhancement of the SF signal in the free-OD and free-OH regions of the isotopic mixtures when compared to the pure compounds (see Figures S2, S3, and S4 in Supporting Information). Second, while the bandwidths remain approximately constant, the peak positions of both the free-OD and the free-OH are red-shifted when compared with the neat liquids (see insets in the SSP and PPP spectra of Figure 7). For the 50:50 H_2O : D_2O mixture shown in Figure 7, the shift is $\sim 23\text{ cm}^{-1}$ and $\sim 8\text{ cm}^{-1}$ for the free-OD and free-OH, respectively.

The free OD region of the liquid/vapor interface of mixtures of D_2O and H_2O has recently been investigated using heterodyne-detected VSFS by Benderskii et al.⁵⁵ Interestingly, two distinct peaks separated by $\sim 17\text{ cm}^{-1}$ were observed in the free-OD stretching region, with only their relative amplitudes changing with isotopic dilution.⁵⁵ The lower and higher

frequency bands were assigned to the free-OD from HOD, and the free-OD from D₂O, respectively. The relative blue shift in the free-OD from D₂O was attributed to be primarily due to an intramolecular coupling with the “donor OD”.⁵⁵ The data presented here indicate a rather different scenario for the hydrophobized solid/liquid interface. First, only a single band is observed in the free-OH and free-OD regions for the 50:50 H₂O:D₂O mixture (Figure 7), where in principle an equal number of free-ODs (OH) from D₂O (H₂O) and HDO are expected (i.e., a D₂O molecules has two potential OD stretches that can be present at the surface as free-OD, while HOD molecules have only one). Second, the peak positions of the free-OD and free-OH modes change depending on the isotopic dilution as summarized in Figure 8 (note that only single bands

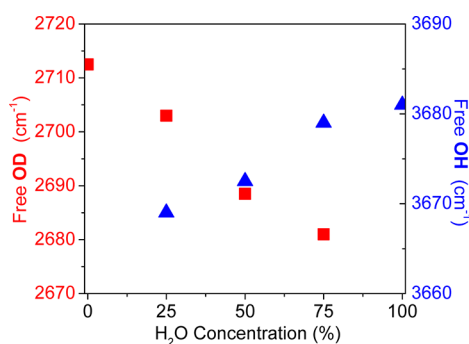


Figure 8. Changes in the peak position of the free-OD (red squares, left scale) and free-OH (blue triangles, right scale) stretching bands as a function of the isotopic dilution.

were also observed for the 25:75 and 75:25 H₂O:D₂O mixtures). The results imply that in contrast to the liquid/vapor interface, the vibrational frequencies of the free-OD (OH) stretch in HOD and D₂O (H₂O) are equivalent when they vibrate next to the hydrophobic monolayer. The interactions (i.e., van der Waals¹⁶) between the dangling OD (OH) and the terminal methyl group of the silane monolayer would appear to have a dominant effect over the intramolecular coupling with the “donor OD (OH)”. Time domain measurements at the hydrophobic solid/water interface, similar to those performed at the liquid/vapor interface,⁵⁶ will be particularly useful to further understand how the intermolecular energy is transferred across the interfacial region. Moreover, following this line of thought, the shift in peak position summarized in Figure 8 implies that the separation between the dangling OD (OH) bonds and the terminal methyl group becomes shorter as the relative isotopic concentration of OD (OH) groups decreases in the mixture.

4. SUMMARY AND CONCLUDING REMARKS

Silica surfaces hydrophobized by alkylsilane self-assembled monolayers are commonly used as model systems to characterize hydrophobic/water interfaces. Although in principle simple to prepare, the quality of the final monolayer depends on a large number of parameters, many of which are interdependent and not always easy to control.^{22–35} These complexities manifest themselves in a certain degree of irreproducibility, even when following apparently identical preparation protocols. In this sense only two different preparation procedures were sufficient to create monolayers with varying degrees of order, as evaluated by the presence of *gauche* defects in the SF spectra. In connection to this latter

point, the high resolution SF spectra obtained here allow resolving two symmetric stretching methylene modes. We suggest they are associated with *gauche* defects at different positions in the silane’s alkyl chain.

The interfacial water structure was found to be dependent on the quality of the prepared hydrophobic layer. For the more ordered monolayers the dangling or free-OH mode from water molecules in direct contact to the methyl groups of the hydrophobic layer was observed to increase, while the broader spectral features associated with hydrogen bonded water molecules located further away from the surface followed the opposite trend. The results obtained give conclusive evidence that, in contrast to previous suggestions,^{13,16} bulk isotropic properties are already present at subnanometer distances from the surface of well ordered hydrophobic monolayers (i.e., the surface induced order in the water structure does not propagate further than just a few ångströms). Moreover, the signal increase observed in the hydrogen bonded water bands for the less well ordered silane monolayers, is a consequence of direct interactions with the underlying fused silica substrate which is made accessible by defects in the hydrophobic monolayer. This interpretation was supported by VSFS and TIR Raman measurements. In the light of the present results, the conclusions reached in recent studies on the adsorption of hydroxide and chloride ions at different pHs to similar hydrophobized silica surfaces¹⁶ may need to be reconsidered. Furthermore, the effect of the silica surface on the interfacial water structure will be even more patent when using fluorinated silanes, which are more reactive to water resulting in a larger number of defects in the monolayer during the grafting procedure.^{17,24}

When comparing with the liquid/vapor and solid/vapor interfaces, the peak positions at the solid/liquid interface of the dangling OH bond from water and the terminal methyl group from the silane, are red-shifted by ~ 20 cm⁻¹ and ~ 3 cm⁻¹, respectively. This provides irrefutable evidence that the molecules in the first monolayer of water are vibrating in direct proximity to the silane monolayer, discarding within our detection limits (i.e., $< 1\%$ of the surface), the presence of air nanobubbles or microparticles^{65,66} at these interfaces. The shift is presumably caused by van der Waals interactions between the water molecules and the silane’s alkyl chains.^{16,17,67}

Contact angle measurements were carried out in an effort to correlate macroscopic measurable parameters with the surface molecular structure. Only the receding contact angles, and in particular those measured using hexadecane, were found to have a connection with the interfacial structure. However, no such correlations were found with the static and advancing angles in water. The apparent link between molecular structure and the receding contact angle, may reflect molecular-scale deformations that only occur in the monolayer when in contact with water for a sufficient length of time.⁶⁸ From a practical perspective, the receding contact angles could be used as a preliminary method to assess the monolayer conformation order.

Finally, isotope dilution experiments with H₂O and D₂O indicate clear differences between the water/vapor and the water/hydrophobic surface interfaces, as evidenced by the presence of a single band in the free-OD (OH) region, which position shifts depending on the isotopic composition. The results suggest that the van der Waals interactions between the terminal methyl group in a hydrophobic monolayer and the dangling OD (OH) bonds gives rise to a different vibrational

coupling mechanism when compared to the liquid/vapor interface.⁵⁵

■ ASSOCIATED CONTENT

■ Supporting Information

VSF spectra of isotope exchange experiments at the neat fused silica/water interface, simulated contour plots showing the influence of the molar fraction of H₂O/D₂O and IR wavelength on the SF intensity, and refractive indexes of water and fused silica at different wavelengths. This material is available free of charge via the Internet at <http://pubs.acs.org/>.

■ AUTHOR INFORMATION

Corresponding Author

*E-mail: tyrode@kth.se. Telephone: +46 8 7909915.

Notes

The authors declare no competing financial interest.

■ ACKNOWLEDGMENTS

Funding by the Swedish Research Council (VR) is gratefully acknowledged. ET acknowledges financial support from the European Community's Marie Curie Reintegration grant, Molecular Structure in Thin Wetting Films, Contract Number FP7-PEOPLE-ERG-2008 No. 239459.

■ REFERENCES

- (1) Chandler, D. *Nature* **2002**, 417, 491.
- (2) Chandler, D. *Nature* **2005**, 437, 640–647.
- (3) Ball, P. *Nature* **2003**, 423, 25–26.
- (4) Jensen, T. R.; Østergaard Jensen, M.; Reitzel, N.; Balashev, K.; Peters, G. H.; Kjaer, K.; Bjørnholm, T. *Phys. Rev. Lett.* **2003**, 90, 086101.
- (5) Mezger, M.; Reichert, H.; Schöder, S.; Okasinski, J.; Schröder, H.; Dosch, H.; Palms, D.; Ralston, J.; Honkimäki, V. *Proc. Natl. Acad. Sci. U.S.A.* **2006**, 103, 18401–18404.
- (6) Mezger, M.; Sedlmeier, F.; Horinek, D.; Reichert, H.; Pontoni, D.; Dosch, H. *J. Am. Chem. Soc.* **2010**, 132, 6735–6741.
- (7) Poynor, A.; Hong, L.; Robinson, I. K.; Granick, S.; Zhang, Z.; Fenter, P. A. *Phys. Rev. Lett.* **2006**, 97, 266101/266101–266101/266104.
- (8) Doshi, D. A.; Watkins, E. B.; Israelachvili, J. N.; Majewski, J. *Proc. Natl. Acad. Sci. U. S. A.* **2005**, 102, 9458–9462.
- (9) Maccarini, M.; Steitz, R.; Himmelhaus, M.; Fick, J.; Tatur, S.; Wolff, M.; Grunze, M.; Janeček, J.; Netz, R. R. *Langmuir* **2006**, 23, 598–608.
- (10) Richmond, G. L. *Chem. Rev.* **2002**, 102, 2693–2724.
- (11) Lambert, A. G.; Davies, P. B.; Neivandt, D. J. *Appl. Spectrosc. Rev.* **2005**, 40, 103–145.
- (12) Bain, C. D. *J. Chem. Soc., Faraday Trans.* **1995**, 91, 1281–1296.
- (13) Du, Q.; Freysz, E.; Shen, Y. R. *Science* **1994**, 264, 826–828.
- (14) Tong, Y.; Tyrode, E.; Osawa, M.; Yoshida, N.; Watanabe, T.; Nakajima, A.; Ye, S. *Langmuir* **2011**, 27, 5420–5426.
- (15) Tyrode, E.; Rutland, M. W.; Bain, C. D. *J. Am. Chem. Soc.* **2008**, 130, 17434–17445.
- (16) Tian, C. S.; Shen, Y. R. *Proc. Natl. Acad. Sci. U.S.A.* **2009**, 106, 15148–15153.
- (17) Hopkins, A. J.; McFearn, C. L.; Richmond, G. L. *J. Phys. Chem. C* **2011**, 115, 11192–11203.
- (18) Brown, M. G.; Walker, D. S.; Raymond, E. A.; Richmond, G. L. *J. Phys. Chem. B* **2003**, 107, 237–244.
- (19) Scatena, L. F.; Brown, M. G.; Richmond, G. L. *Science* **2001**, 292, 908–912.
- (20) Ye, S.; Nihonyanagi, S.; Uosaki, K. *Phys. Chem. Chem. Phys.* **2001**, 3, 3463–3469.
- (21) Scatena, L. F.; Richmond, G. L. *J. Phys. Chem. B* **2001**, 105, 11240–11250.
- (22) Sagiv, J. *J. Am. Chem. Soc.* **1980**, 102, 92–98.
- (23) Offord, D. A.; Griffin, J. H. *Langmuir* **1993**, 9, 3015–3025.
- (24) Brzoska, J. B.; Azouz, I. B.; Rondelez, F. *Langmuir* **1994**, 10, 4367–4373.
- (25) Wang, R.; Guo, J.; Baran, G.; Wunder, S. L. *Langmuir* **2000**, 16, 568–576.
- (26) Desbief, S.; Patrone, L.; Goguenheim, D.; Guerin, D.; Vuillaume, D. *Phys. Chem. Chem. Phys.* **2011**, 13, 2870–2879.
- (27) McGovern, M. E.; Kallury, K. M. R.; Thompson, M. *Langmuir* **1994**, 10, 3607–3614.
- (28) Bierbaum, K.; Grunze, M.; Baski, A. A.; Chi, L. F.; Schrepp, W.; Fuchs, H. *Langmuir* **1995**, 11, 2143–2150.
- (29) Le Grange, J. D.; Markham, J. L.; Kurkjian, C. R. *Langmuir* **1993**, 9, 1749–1753.
- (30) Richter, A. G.; Yu, C. J.; Datta, A.; Kmetko, J.; Dutta, P. *Phys. Rev. E* **2000**, 61, 607–615.
- (31) Vallant, T.; Kattner, J.; Brunner, H.; Mayer, U.; Hoffmann, H. *Langmuir* **1999**, 15, 5339–5346.
- (32) Tripp, C. P.; Hair, M. L. *Langmuir* **1992**, 8, 1120–1126.
- (33) Liu, Y.; Wolf, L. K.; Messmer, M. C. *Langmuir* **2001**, 17, 4329–4335.
- (34) Iimura, K.-i.; Nakajima, Y.; Kato, T. *Thin Solid Films* **2000**, 379, 230–239.
- (35) Lagutchev, A. S.; Song, K. J.; Huang, J. Y.; Yang, P. K.; Chuang, T. J. *Chem. Phys.* **1998**, 226, 337–349.
- (36) Liljeblad, J. F. D.; Tyrode, E. *J. Phys. Chem. C* **2012**, 116, 22893–22903.
- (37) Greene, P. A.; Bain, C. D. *Spectrosc. Eur.* **2004**, 16, 8–15.
- (38) Woods, D. A.; Bain, C. D. *Analyst* **2012**, 137, 35–48.
- (39) Du, Q.; Freysz, E.; Shen, Y. R. *Phys. Rev. Lett.* **1994**, 72, 238–241.
- (40) Ostroverkhov, V.; Waychunas, G. A.; Shen, Y. R. *Chem. Phys. Lett.* **2004**, 386, 144–148.
- (41) Ostroverkhov, V.; Waychunas, G. A.; Shen, Y. R. *Phys. Rev. Lett.* **2005**, 94, 046102/046101–046102/046104.
- (42) Yeganeh, M. S.; Dougal, S. M.; Pink, H. S. *Phys. Rev. Lett.* **1999**, 83, 1179–1182.
- (43) Jena, K. C.; Hore, D. K. *J. Phys. Chem. C* **2009**, 113, 15364–15372.
- (44) Sovago, M.; Kramer Campen, R.; Bakker, H. J.; Bonn, M. *Chem. Phys. Lett.* **2009**, 470, 7–12.
- (45) Iler, R. K. *The chemistry of silica: solubility, polymerization, colloid and surface properties, and biochemistry*; Wiley: New York, 1979.
- (46) Ong, S.; Zhao, X.; Eiseenthal, K. B. *Chem. Phys. Lett.* **1992**, 191, 327–335.
- (47) Nihonyanagi, S.; Ishiyama, T.; Lee, T.-k.; Yamaguchi, S.; Bonn, M.; Morita, A.; Tahara, T. *J. Am. Chem. Soc.* **2011**, 133, 16875–16880.
- (48) Tyrode, E.; Niga, P.; Johnson, M.; Rutland, M. W. *Langmuir* **2010**, 26, 14024–14031.
- (49) Guyot-Sionnest, P.; Hunt, J. H.; Shen, Y. R. *Phys. Rev. Lett.* **1987**, 59, 1597–1600.
- (50) Bell, G. R.; Bain, C. D.; Ward, R. N. *J. Chem. Soc., Faraday Trans.* **1996**, 92, 515–523.
- (51) Tyrode, E.; Hedberg, J. J. *J. Phys. Chem. C* **2012**, 116, 1080–1091.
- (52) Tyrode, E.; Johnson, C. M.; Kumpulainen, A.; Rutland, M. W.; Claesson, P. M. *J. Am. Chem. Soc.* **2005**, 127, 16848–16859.
- (53) Walker, D. S.; Hore, D. K.; Richmond, G. L. *J. Phys. Chem. B* **2006**, 110, 20451–20459.
- (54) Walker, D. S.; Richmond, G. L. *J. Phys. Chem. C* **2007**, 112, 201–209.
- (55) Stipokin, I. V.; Weeraman, C.; Pieniazek, P. A.; Shalhout, F. Y.; Skinner, J. L.; Benderskii, A. V. *Nature* **2011**, 474, 192–195.
- (56) Zhang, Z.; Piatkowski, L.; Bakker, H. J.; Bonn, M. *Nature Chem.* **2011**, 3, 888–893.
- (57) Zhao, X.; Kopelman, R. J. *J. Phys. Chem.* **1996**, 100, 11014–11018.
- (58) Persson, C. M.; Claesson, P. M.; Lunkenheimer, K. J. *Colloid Interface Sci.* **2002**, 251, 182–192.
- (59) Stubenrauch, C.; Rojas, O. J.; Schlarmann, J.; Claesson, P. M. *Langmuir* **2004**, 20, 4977–4988.

- (60) Kjellin, U. R. M.; Claesson, P. M.; Linse, P. *Langmuir* **2002**, *18*, 6745–6753.
- (61) Gaber, B. P.; Peticolas, W. L. *Biochim. Biophys. Acta, Biomembr.* **1977**, *465*, 260–274.
- (62) Laibinis, P. E.; Nuzzo, R. G.; Whitesides, G. M. *J. Phys. Chem.* **1992**, *96*, 5097–5105.
- (63) Walker, D. S.; Richmond, G. L. *J. Phys. Chem. C* **2007**, *111*, 8321–8330.
- (64) Raymond, E. A.; Tarbuck, T. L.; Brown, M. G.; Richmond, G. L. *J. Phys. Chem. B* **2003**, *107*, 546–556.
- (65) James, R. T. S.; Detlef, L. *J. Phys.: Condens. Matter* **2011**, *23*, 133001.
- (66) Craig, V. S. J. *Soft Matter* **2011**, *7*, 40–48.
- (67) Vácha, R.; Zangi, R.; Engberts, J. B. F. N.; Jungwirth, P. *J. Phys. Chem. C* **2008**, *112*, 7689–7692.
- (68) Israelachvili, J. N. *Intermolecular and Surface Forces*, 3rd ed.; Elsevier: Oxford, U.K., 2011.